# Singlet Deuterons ($\hat{d}$) from ($p$, $\hat{d}$) Reactions*

B. L. COHEN, E. C. MAY,† T. M. O'KEEFE,‡ AND C. L. FINK
*University of Pittsburgh, Pittsburgh, Pennsylvania 15213*

(Received 3 October 1968)

Singlet deuterons $\hat{d}$ (i.e., a neutron-proton system in the $S=0$, $T=1$ virtual state) are treated as particles emitted from nuclear reactions. A method for detecting them by $n$-$p$ coincidence time-of-flight techniques is described. ($p$, $\hat{d}$) reactions induced by 12-MeV protons on $Li^7$ and $Be^9$, and by 17-MeV protons on $Be^9$, $C^{13}$, $Mg^{25}$, and $Sn^{117}$ are investigated. In the lighter elements, angular distributions of $\hat{d}$ are measured and compared with those of deuterons from analogous ($p$, $d$) reactions, and the ratios $R=\sigma(p, d)/\sigma(p, \hat{d})$ are determined. Semiquantitative comparisons with theory indicate reasonable agreement. In $Mg^{25}$ and $Sn^{117}$, no ($p$, $\hat{d}$) reactions could be detected, although they are expected to be observable at least in $Sn^{117}$.

## INTRODUCTION AND OUTLINE OF METHOD

DEUTRONS have historically played an important part in nuclear reaction studies; ($d$, $p$), ($d$, $n$), ($d$, $He_3$), ($p$, $d$), ($\alpha$, $d$), etc., reactions have been among our most useful tools for investigating nuclear structure. A deuteron is a neutron-proton system in its lowest $T=0$, $S=1$ state, and it is well known that this system has a closely related $T=1$, $S=0$ state which is commonly referred to as the "singlet deuteron." It therefore seems interesting to investigate the role of the singlet deuteron—we will refer to it as $\hat{d}$—in nuclear reactions. The great complication in doing this is that the $\hat{d}$ is unstable by about 60 keV, so that these investigations must involve detection of the neutron and proton decay products. Temmer[1] attempted to study $\hat{d}$'s by detection of the neutrons and protons separately, but as we shall see, coincidence detection is an absolute necessity. The Rice group[2] found evidence for $\hat{d}$'s in their coincidence experiments on $p+d\rightarrow p+p+n$, but they did not give results on $\hat{d}$'s as a particle; for example, they did not discuss their energy or angular distributions.

In this paper we will attempt to think of $\hat{d}$'s as particles emitted from nuclear reactions, and investigate to what extent such reactions can be treated as analogous to reactions in which emitted particles are stable. If such treatments are successful both experimentally and theoretically, $\hat{d}$ would be a very useful new particle. For example, advantage could be taken of its $T=1$ character to excite states which cannot be reached in analogous reactions with ordinary ($T=0$) deuterons.

Reactions involving unstable particles are not new to nuclear physics. For example, ($\alpha$, $Be^8$) reactions were studied several years ago at the University of Washington,[3] even though $Be^8$ nuclei have a lifetime of about $3\times10^{-16}$ sec before breaking up into two $\alpha$ particles with 90 keV of energy release. However, even $3\times10^{-16}$ sec is a long time on a nuclear scale—many orders of magnitude longer than the characteristic nuclear time $\tau_0$, the time for a nucleon to traverse a nuclear radius. Equivalently, it corresponds through the Uncertainty Principle to a width of about 2 eV which is orders of magnitude less than typical energies of nuclear reaction products. It is thus not surprising that reactions involving a $Be^8$ product can be treated to a very good approximation as though $Be^8$ were stable.

For $\hat{d}$, on the other hand, things are not so simple. The lifetime, in so far as it has a meaning, is of the order of $\tau_0$, and the energy width is correspondingly large. This difference manifests itself not only in the theoretical interpretation, but also in the experimental problems of detecting the particles. In the $Be^8$ case, we may write

$$\begin{aligned} &E_{Be^8}=E_{\text{incident}}+Q-E_{\text{recoil}}=\text{a known const}\\ &\quad=\tfrac{1}{2}M_{Be^8}v^2,\\ &E_{BU}=90\text{ keV}=\tfrac{1}{2}\mu(2u)^2=\tfrac{1}{2}(m_\alpha/2)4u^2=mu^2, \quad (1)\\ &\mathbf{v}_\alpha=\mathbf{v}+\mathbf{u},\\ &E_\alpha=\tfrac{1}{2}m_\alpha v_\alpha^2, \end{aligned}$$

where $Q$ is the energy release in the original reaction, $\mathbf{v}$ the velocity of the $Be^8$ nucleus, $E_{BU}$ is the energy released in the breakup, $\mathbf{u}$ and $-\mathbf{u}$ are the velocities of the $\alpha$ particles in the center-of-mass system of $Be^8$, $\mu$ is the reduced mass, and other symbols have self-evident meanings. Since $v$ is ordinarily very much larger than $u$, the two $v_\alpha$ are nearly equal regardless of the angle $\phi$ between $\mathbf{v}$ and $\mathbf{u}$. This means that the two $\alpha$ particles are very strongly correlated both in energy and direction, which allows for easy and efficient detection.

For the $\hat{d}$ case, on the other hand, the most general equations we can write are

$$\begin{aligned} &E_{\hat{d}}+E_{BU}=E_{\text{incident}}+Q-E_{\text{recoil}}\simeq E_0,\text{ a known const},\\ &\quad E_{\hat{d}}=\tfrac{1}{2}(2m)v^2=mv^2,\\ &E_{BU}=\tfrac{1}{2}\mu(2u)^2=\tfrac{1}{2}(\tfrac{1}{2}m)4u^2=mu^2, \quad (2)\\ &\mathbf{v}_n=\mathbf{v}+\mathbf{u},\\ &E_n=\tfrac{1}{2}mv_n^2=\tfrac{1}{2}m[(v+u\cos\phi)^2+(u\sin\phi)^2], \end{aligned}$$

* Supported by National Science Foundation.
† Present address: University of California, Davis, Calif.
‡ Present address: Department of Health, Education and Welfare, Washington, D.C.
[1] G. M. Temmer, Bull. Am. Phys. Soc. 9, 108 (1964); Argonne National Laboratory Report No. ANL-6848, 1964 (unpublished), p. 180.
[2] W. D. Simpson, Ph.D. thesis, Rice University, 1965 (unpublished).
[3] R. E. Brown, J. S. Blair, D. Bodansky, N. Cue, and C. K. Kavaloski, Phys. Rev. 138, B1394 (1965).

where $m$, $\mathbf{v}_n$, and $E_n$ are the mass, velocity, and energy of a neutron or proton from the breakup, respectively. These equations differ from (1) in that $E_{BU}$ cannot be specified accurately since it has a very wide probability distribution. One approach to determining this distribution is to assume it to be proportional to the "density-of-states" function of Phillips, Griffy, and Biedenharn.[4,5] An example of this function, whose calculation is outlined in Appendix A, is shown in Fig. 1. We see there that the most probable value of $E_{BU}$ is indeed about 60 keV, but it has a very wide distribution, with values of several MeV having reasonably large probabilities. Thus, we no longer have the simple situation where $v$ is much less than $u$, whence the neutron and proton are not strongly correlated in energy or direction. This greatly complicates the detection problem.

In order to minimize this complication, we employ a detection system in which the neutron and proton are detected in coincidence at the same angle—that is, their detectors are on the same line from the target. This immediately assures that the $\hat{d}$ was emitted at this angle, for otherwise momentum conservation would not allow both particles to reach their detectors. It furthermore requires that the angle $\phi$ between $\mathbf{v}$ and $\mathbf{u}$ be near 0° (or 180°). How near to these it must be, which we designate $\phi_m$, is clearly determined by $E_{BU}$—for large values of $E_{BU}$ it must be very near indeed, so $\phi_m$ is small; but for small $E_{BU}$, $\phi_m$ can be reasonably large; for $E_{BU}$ near zero, both particles reach their detectors regardless of the value of $\phi$. Since any value of $\phi$ has an intrinsic probability proportional to $\sin\phi$ from integration over azimuthal angles, the probability that $\phi$ will be less than $\phi_m$, as found by simple integration, is $\frac{1}{2}(1-\cos\phi_m)\simeq\frac{1}{4}\phi_m^2$. This detection method, therefore, heavily favors

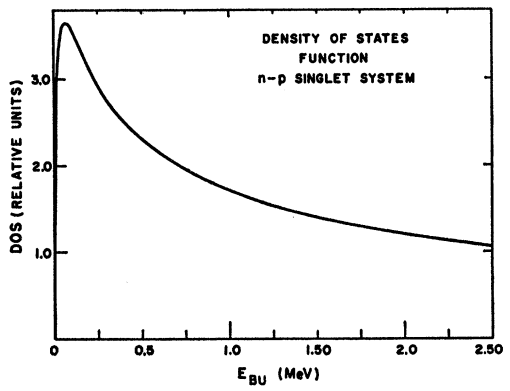


FIG. 1. Density-of-states function. This was calculated as described in Appendix A, based on the theory of Phillips, Griffy, and Biedenharn in Refs. 4 and 5. See also Ref. 2.

[4] G. C. Phillips, T. A. Griffy, and L. C. Biedenharn, Nucl. Phys. **21**, 327 (1960).

[5] The density-of-states function of Ref. 4 was slightly modified to take into account the density of states in the continuum of the $\hat{d}$ as described in Appendix A.

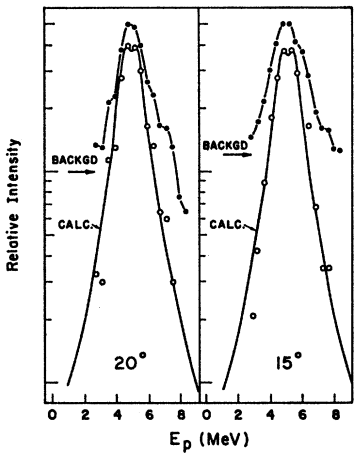


FIG. 2. Data on $(p, \hat{d})$ induced by 12-MeV protons on $Be^9$, from Ref. 6.

breakups in which $E_{BU}$ is small. This, plus the fact that small $E_{BU}$ are already favored by the probability distribution in Fig. 1, means that *among events being detected* $E_{BU}$ is much less than $E_{\hat{d}}$ whence, from (2)

$$E_n\simeq\tfrac{1}{2}E_0. \tag{3}$$

Thus the observed energy distribution of neutrons or protons is sharply peaked at one-half their maximum energies. The shape of this peak may readily be calculated (cf. Appendix $A$) and compared with experiment. Such a comparison is shown in Fig. 2 which was taken from a preliminary report on this work.[6] We see there that the peak is reasonably sharp which allows differentiation from other processes in which neutrons and protons are emitted in coincidence.

It is important to point out here that there is still a big difference between this method of detecting $\hat{d}$'s and the detection of $Be^8$ nuclei. In the latter case, if two detectors of reasonable solid angle could be placed at the same angle, virtually all $Be^8$ nuclei emitted at that angle would be detected. On the other hand, in the great majority of $\hat{d}$ breakups, $E_{BU}$ is large and $\phi$ is not near 0°, whence the neutron and proton come off at angles diverging widely and in opposite directions from the original angle of emission of the $\hat{d}$. In such cases $E_n$ is not near $\frac{1}{2}E_0$; this does not disturb the peak at $E_n=\frac{1}{2}E_0$ since both particles are not simultaneously detected in our experimental arrangement, but the fact that most $\hat{d}$ events end up that way means that our detection efficiency is low.

Table I gives the $\hat{d}$ detection efficiency calculated by the methods of Appendix A for various solid angles subtended by the neutron detector which is assumed to subtend a much larger solid angle than the proton detector. These efficiencies are generally only a few percent, and they must be multiplied by the ~20%

[6] B. L. Cohen, E. C. May, and T. M. O'Keefe, Phys. Rev. Letters **18**, 962 (1967).

TABLE I. $\bar{d}$ detection efficiency for various solid angles of the neutron detector. The $\bar{d}$ energy is 10 MeV.

| $\Omega_n$ (sr) | 0.0063 | 0.025 | 0.050 | 0.100 | 0.19 |
|---|---|---|---|---|---|
| $\bar{d}$ efficiency (%) | 0.6 | 2.2 | 4.3 | 7.5 | 11.4 |

detection efficiency of the neutron detector for neutrons that reach it. The over-all detection efficiency for $\bar{d}$ is, thus, only about 1%.

In applying these techniques to the detection of $\bar{d}$'s from nuclear reactions, one is tempted immediately to investigate cases where the $T=1$ nature of the $\bar{d}$ is important, as for example in $(\alpha, \bar{d})$ reactions. Unfortunately, the energy available at this laboratory is insufficient for this. Some attempts were made to study $(d, \bar{d})$ reactions on $T=0$ targets leading to $T=1$ states, but these cases have both experimental difficulties and problems arising from nuclear structure peculiarities—for example, they are very weakly excited in $(p, p')$ reactions.

It was therefore decided to study $(p, \bar{d})$ reactions. These have the advantage that the nuclear reaction and structure theories involved are well understood, and in fact are the same as those applicable in the analogous $(p, d)$ reactions. In fact, one can make a rough *a priori* estimate of the cross-section ratio, $R$, of $(p, d)/(p, \bar{d})$:

(a) In the usual formula for the cross section for a pickup reaction there is a term $(2S+1)$ where $S$ is the spin of the emitted particle. This factor is 3 for $(p, d)$ and 1 for $(p, \bar{d})$, so it contributes a factor 3 to $R$.

(b) In the matrix element for the transition, the interaction is $V_{np}$, the free neutron-proton interaction potential; this is 0.63 times as large in a singlet as in a triplet state.[7] Since the matrix element is squared, this contributes a factor 2.5 to $R$.

(c) The $Q$ value of a $(p, \bar{d})$ reaction is less by 2.2 MeV than that for the corresponding $(p, d)$ reaction. This should decrease the cross section for the former by a factor of at least about 1.3, and perhaps much larger, depending on the energies of the situation. It is thus expected that the ratio $R$ should be at least 10, and in some cases as much as 20 or even more. The result in Ref. 6 when corrected for an error in the efficiency calculation was $R=13.0$. One of the aims of this work is to measure $R$ by measuring the relative intensities of $d$ and $\bar{d}$ in analogous transitions.

Of the above listed factors only (c) has an effect on the angular distribution. In simple Born approximation, the angular distribution is determined by the momentum transfer $q$ which is

$$q^2=k_p^2+k_d^2-2k_pk_d\cos\theta.$$

If $k_p$ and $k_d$ are of about the same magnitude, we may write

$$k_p=k; \qquad |k_d|=|k|+\Delta$$

whence, ignoring terms of order $\Delta^2$,

$$q\simeq 2k^2+2k\Delta-2k^2\cos\theta-2k\Delta\cos\theta$$
$$=2k(k+\Delta)(1-\cos\theta)$$
$$=2k_pk_d(1-\cos\theta).$$

A peak in an angular distribution occurs for a given value of $q$; since $k_d$ is less for $\bar{d}$ than for $d$, $(1-\cos\theta)$ must be larger, whence $\theta$ must be larger. Thus, the angular distribution of $\bar{d}$ should be similar to that for $d$ except that peaks should be shifted to slightly larger angles. Such an effect was reported in Ref. 6, and is to be expected in general.

In this paper we will first describe the experimental techniques and then present the results of measurements on $(p, \bar{d})$ reactions on various targets. These include measurements of angular distributions of both $\bar{d}$'s and $d$'s, and determinations of $R$.

We fully realize that thinking of the singlet deuteron as a particle is unnecessary and may even be misleading; the reactions may also be considered as $(p, pn)$ reactions with final-state interactions. The results will, therefore, also be presented in a way that is useful for theorists using the latter approach.

## EXPERIMENTAL

The experiment involves irradiating a target with energetic protons and detecting the neutrons and protons emitted from $(p, pn)$ reactions in coincidence while simultaneously measuring their energies. Protons are detected with surface barrier detectors and their energies are determined from pulse-height analysis. Neutrons are detected with a plastic scintillator, and their energies are determined by time of flight from a measurement of the difference in time of arrival of the neutrons and protons in their respective detectors.

The incident beam from the University of Pittsburgh three stage Van de Graaff accelerator enters a thin-walled 12-in.-diam reaction chamber through a $\frac{1}{4}$-in.-diam slit, passes through the target at the center of the chamber, and travels about 20 ft down an evacuated pipe to an insulated collector shielded from the remainder of the apparatus by concrete blocks. The current on the slit is monitored, and beam steering and focussing devices are set to minimize its ratio to the collector current. As a result of these precautions and the use of relatively thick targets (typically 3 mg/cm$^2$), the majority of counts in the neutron detector originate from the target. The proton detector is well shielded

[7] M. A. Preston, *Physics of the Nucleus* (Addison-Wesley Publishing Company, Inc., Reading, Mass., 1963). The authors are greatly indebted to Dr. K. Nagatani for pointing out this factor.

from the entrance slit, and target holders with large open areas are used, so essentially all counts reaching the proton detector come from the target. The beam is monitored by a surface barrier detector measuring elastically scattered protons at a deflection angle of 30° out of the reaction plane. Incident beam currents are limited by the total count rate in the proton and neutron detectors which are each kept below 40 000 counts/sec; typical beam currents are 5 to 20 nA.

The electronics arrangement is shown in Fig. 3. The neutron detector is a $3\frac{1}{2}$-in.-diam, $\frac{3}{4}$-in.-thick Pilot B scintillator machined to fit on an Amperex 58 AVP photomultiplier. The anode signal is shaped to be bipolar by a shorted transmission line and fed into a fast zero-crossover discriminator. The discrimination level is set by an attenuator at the input to about $\frac{1}{4}$ of the Compton edge for $Cs^{137}$ $\gamma$ rays; this corresponds to about 110 keV for $\gamma$ rays and about 850 keV for neutrons. The discriminator output is then used as the start pulse for a time to pulse-height converter (TPHC).

The proton detector consists of a 200-$\mu$ thick front ($\Delta E$) detector and a back (E) detector thick enough to stop the full energy protons. The timing signal is taken from the $\Delta E$ detector and fed into an FET source follower. The output is amplified with fast amplifiers and used to trigger a leading-edge discriminator whose output serves as the "stop" signal for the TPHC. As the TPHC does not work properly at high input count rates, it is gated by a coincidence circuit which fires only when signals occur in both discriminators within a 100-nsec time interval; this reduces the count rate to a few per second. The TPHC output is amplified and fed into a two-dimensional pulse-height analyzer (2DPHA).

The proton energy is obtained by adding the $\Delta E$ and $E$ pulses after suitable pulse shaping and amplification. In order to avoid inserting high count rates into the 2DPHA and thereby suffering large dead-time losses, the summed pulse is passed through a linear gate which is again gated by the 100-nsec coincidence circuit; pulses getting through the linear gate are fed into the 2DPHA. Delays are introduced where necessary to achieve proper timing as shown in Fig. 3.

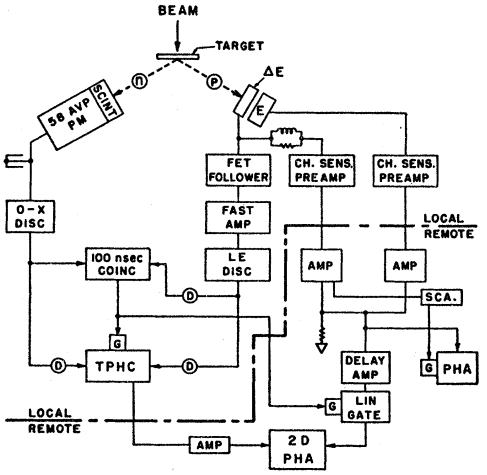


FIG. 3. Experimental arrangement as described in text. Encircled $D$ indicates a delay cable, and a boxed $G$ indicates a gate.

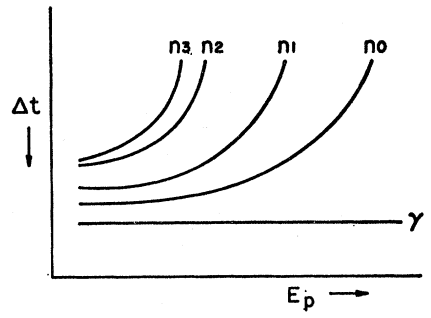


FIG. 4. Plots of $\Delta t$, difference in time of arrival of neutrons and protons at their respective detectors, versus $E_p$, the energy of the proton. This is the display on the two-dimensional pulse-height analyzer. $n_0$ is the locus of points corresponding to events in which the final nucleus is left in its ground state, $n_1$, $n_2$,$\cdots$ are the same for excited states, and the line labeled $\gamma$ is the locus of $(p$-$\gamma)$ coincident events.

The output of the 2DPHA gives a plot of $\Delta t$ versus $E_p$ as shown schematically in Fig. 4. Events in which the sum of the neutron and proton energies correspond to the final nucleus being left in its ground-state fall along the curve labeled $n_0$; where the final nucleus is left in its first, second, etc., excited states, the kinematic locus is the curve labeled $n_1$, $n_2$, etc., $\gamma$ rays detected by the neutron detector in coincidence with protons occur at the same time for all values of $E_p$, so these events fall along the horizontal line labeled $\gamma$. Proton energies are calibrated with a precision pulser, and the time axis is calibrated by inserting known delays. Typical runs use about 400 keV per channel in $E_p$ and 0.7 nsec per channel in time. In all cases, ridges of increased intensity fall at the calculated places.

The principal experimental difficulties arise from the need for reasonable neutron energy resolution, which depends in turn on the length-of-flight path and the time resolution. The time jitter in the neutron detection system is about 0.8 nsec; it is limited principally by the transit time difference between the center and outside of the photomultiplier and by the time of flight of neutrons through the scintillation crystal. Much better time resolutions were achieved in tests with small crystals, but it was decided that this improvement would not be worth the sacrifice in detection efficiency. In any case, equivalent results can be obtained with longer flight paths. With detector diameters much larger than $3\frac{1}{2}$-in., time resolution deteriorates rapidly.

The time jitter introduced by the proton detection

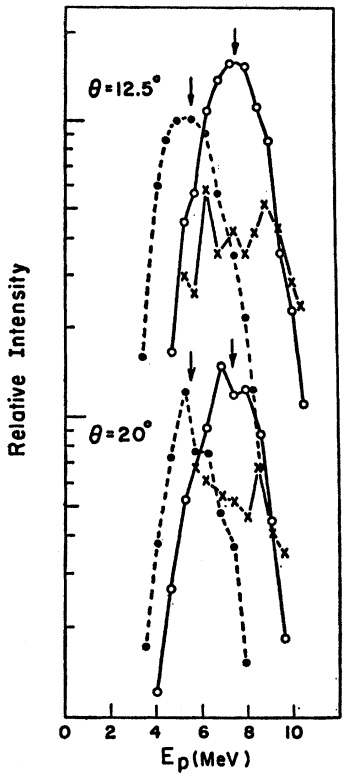


FIG. 5. Typical data from $(p, d)$ reactions on $Be^9$ induced by 17-MeV protons. Open circles are for ground-state transitions, filled circles are for transitions leaving $Be^8$ in its 2.9-MeV excited state, and crosses are opposite-sides data for the ground-state transition. Upper and lower parts of figure are for data obtained at 12.5 and 20°, respectively.

system $\delta t$ is

$$\delta t = \frac{N}{dV/dt} \simeq \frac{N}{V_m/\tau}, \tag{4}$$

where $dV/dt$ is the rate of rise of the voltage pulse at the amplifier input, $N$ is the noise at that point, $V_m$ is the pulse height, and $\tau$ is the rise time. But

$$V_m = Q/C \propto \delta E/(C_D+C_S), \tag{5}$$

where $Q$ is the total charge collected which is proportional to the energy loss in the $\Delta E$ detector, $\delta E$; and $C_D$ and $C_S$ are the detector and stray capacitances. Also, for a fully depleted detector[8]

$$\tau \simeq d/\mu_e E \simeq d^2/\mu_e V_B, \tag{6}$$

where $d$ is the detector thickness, $\mu_e$ is the electron mobility, and $V_B$ is the bias voltage. Combining (4)–(6) gives

$$\delta t \propto N d^2 (C_D+C_S)/\mu_e V_B \delta E. \tag{7}$$

On first examination of (7) one gets the impression that a very thin $\Delta E$ detector would be advantageous in that it minimizes $d$. However, if it is very thin, $C_S \ll C_D \propto 1/d$, $\delta E \propto d$, and $V_B$ is roughly $\propto d$, so the $d^2$ in the numerator is more than canceled by a $d^3$ in the denominator. It is therefore somewhere near optimum to choose $d$ large enough to stop protons of the average energy where good time resolution is needed. This eliminates the factor arising from $\delta E$, and in view of the fact that $C_S$ is at least comparable to $C_D$, gives a smaller $\delta t$ from (7) than would be obtained for larger $d$. From these considerations, a $\Delta E$ detector of 200-$\mu$ thickness was chosen. There is a very important economic corollary in this choice; the detector used for timing must be biased[8] to about twice the rated $V_B$ which shortens its useful life, so it is preferable to do this with a low cost detector; detector costs are a minimum at about 200-$\mu$ thickness.

In the early part of these experiments there were difficulties with amplifier noise causing $\delta t$ to be greater than 1 nsec. This was then reduced by cooling the detector with dry ice to increase $\mu_e$, but later improvements in amplifier noise levels eliminated this necessity by reducing $\delta t$ to $<0.5$ nsec.

The over-all time resolution of the entire system was about 1.3 nsec in the earliest experiments and about 0.9 nsec in the latest. Neutron flight paths varied from 19–50 cm depending on the needs of neutron energy and angular resolution. There was no loss in efficiency of proton detection (due to failure to fire the timing discriminator) above 1 MeV. After the most recent improvements, this low-energy limit has been reduced to $\sim\frac{1}{4}$ MeV.

Typical running times at a single angle vary between 30–150 min. The memory of the 2DPHA is then dumped on magnetic tape. The latter is computer processed to give, for each $E_p$ channel in the region of interest, a plot of counts per channel versus $\Delta t$ and a running sum. Locations of peaks on these plots are checked to see that they conform to the calculated positions of ridges in Fig. 4; background due to accidentals is estimated from regions far away from peaks and subtracted from the areas under the peaks. Corrections for the neutron detection efficiency of the plastic scintillator, as calculated from the free neutron-proton scattering cross section, are then applied. The results are finally plotted as intensity versus $E_p$ for each ridge in Fig. 4. Figure 2 gives examples of such plots.

Simultaneously with the acquisition of data on singlet deuterons, data are accumulated on ordinary (triplet) deuterons from analogous $(p, d)$ reactions with another multichannel pulse-height analyzer (PHA). This receives the summed energy pulse and is gated by a single-channel analyzer (SCA) acting on amplified pulses from the $\Delta E$ detector and set to detect deuterons. Since the range of deuteron energies needed is quite small, there is no need for sophisticated particle

[8] B. L. Cohen and C. L. Fink, Nucl. Instr. Methods **57**, 93 (1967).

identification techniques, although it is sometimes found necessary to obtain a $\Delta E$ versus $E+\Delta E$ two-dimensional display in order to set the window of the single-channel analyzer. Dead times on the PHA are frequently quite appreciable; they are corrected for by feeding pulses from the monitor into the external clock input of the analyzer, so deuteron counts per monitor count are obtained directly.

## RESULTS

### 1. $Be^9(p, \vec{d})Be^8$ (17 MeV)

The $Be^9(p, \vec{d})Be^8$ reaction was studied with an incident proton energy of 17 MeV, and transitions to both the ground and first excited (2.9-MeV) states of $Be^8$ were observed. Figure 5 shows some typical spectra (at 12.5 and 20°). The curves through the circled points correspond to the ground-state transition while the dashed curves correspond to the transition to the first excited state. The vertical arrows indicate the position that corresponds to $\frac{1}{2}E_0$. In all cases the peak has the right width and occurs in the appropriate place as governed by the kinematics and the reaction $Q$ values.

One method of estimating the contribution of ordinary $(p, pn)$ reactions is to make measurements with the neutron and proton detectors at equal angles relative to the incident beam but on opposite sides of it.[6] If, as is usually assumed, $(p, pn)$ reactions are inelastic scattering followed by neutron evaporation,

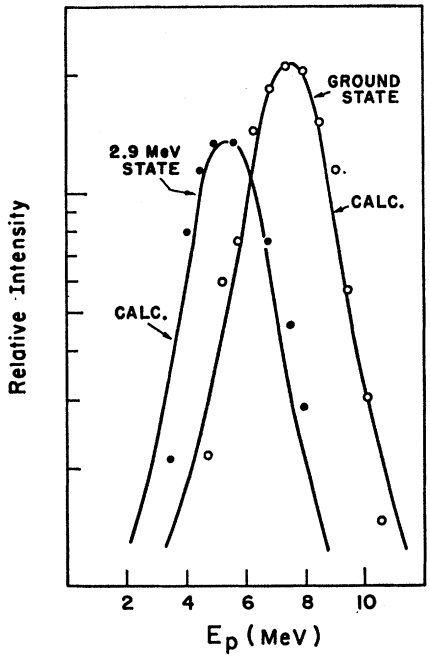


FIG. 6. Comparison between experimental (after subtraction of background as estimated from opposite-side data) and calculated (as described in Appendix A) proton energy spectra. This example is from $Be^9$ $(p, \vec{d})$ at 12.5°.

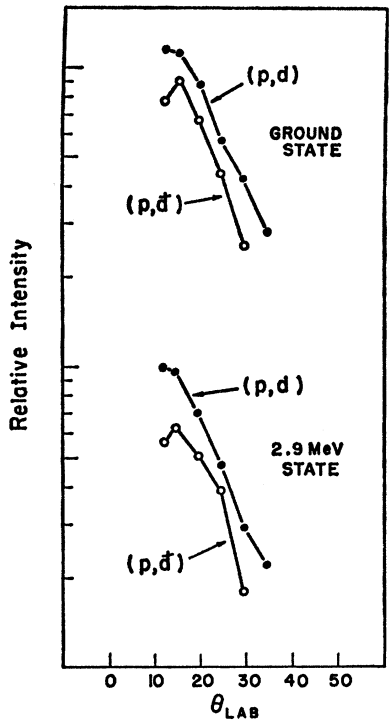


FIG. 7. Angular distribution of $d$ and $\vec{d}$ from $(p, d)$ and $(p, \vec{d})$ reactions on $Be^9$ induced by 17-MeV protons. Results are for transitions to the ground and 2.9-MeV excited states of $Be^8$ as labeled.

approximately equal numbers of events would be observed in this arrangement (which we refer to as "opposite sides") as in the regular arrangement for $\vec{d}$ detection with the neutron detector directly behind the proton detector (which we refer to as "same side"). The crosses in Fig. 5 indicate the data taken on opposite sides of the beam. There is no indication of a well-defined peak in this $(p, pn)$ "background." An example of the comparison between the calculated (as described in Appendix A) and measured energy distributions after subtraction of this background is shown in Fig. 6. The agreement is quite satisfactory for both the ground- and excited-state transitions.

The angular distributions obtained from these data are shown in Fig. 7 by the open circles. The solid points show the angular distribution of deuterons from the analogous $Be^9(p, d)Be^8$ reactions. The curves are drawn on an arbitrary intensity scale, but may be compared for their shape. There is close agreement between the $(p, \vec{d})$ and $(p, d)$ angular distributions; however, the peak is shifted towards a larger angle for the $(p, \vec{d})$ distribution, as expected.

The ratio $R$ between the cross sections for corresponding $(p, d)$ and $(p, \vec{d})$ reactions is listed in Table II It is noteworthy that this ratio is abeut the same as that at 12 MeV[6] which is also listed in Table II.

TABLE II. Summary of results on $(p, d)/(p, \bar{d})$ ratio. The $\Omega_n$ and $\bar{d}$ detection efficiencies are included to make theoretical analysis possible by other theories than that used. Raw count ratios are $R/(\bar{d}$ efficiency).

| Target | $E$ (MeV) | $Q$ (MeV) | $\Omega_n$ | $\bar{d}$ efficiency (%) | $R=\sigma(p,d)/\sigma(p,\bar{d})$ |
|---|---|---|---|---|---|
| $Li^7$ | 12.0 | −7.25 | 0.050 | 3.0 | 41.0 |
| $Be^9$ | 12.0 | −1.67 | 0.049 | 4.2 | 13.0 |
| $Be^9$ | 17.0 | −1.67 | 0.025 | 2.8 | 11.8 |
| $Be^9$ | 17.0 | −4.57 | 0.025 | 2.5 | 14.1 |
| $C^{13}$ | 17.0 | −4.95 | 0.10 | 9.5 | 17 |
| $Mg^{25}$ | 17.0 | −7.33 | 0.049 | 4.2 | >10 |
| $Mg^{25}$ | 17.0 | −8.70 | 0.049 | 4.0 | >5 |
| $Sn^{119}$ | 17.0 | −6.48 | 0.17 | 11.6 | >50 |

A long standing mystery concerning the $Be^9(p, d)$ reactions arises from the fact that the angular distribution is essentially the same over a very wide energy range.[9] While DWBA fits can easily be made at any one energy, parameters must be changed to fit the data at each energy. The angular distributions from $(p, \bar{d})$ given here may help to elucidate this mystery. They are closely similar at 12 and 17 MeV, but differ from the $(p, d)$ angular distributions which are also similar to each other at the two energies

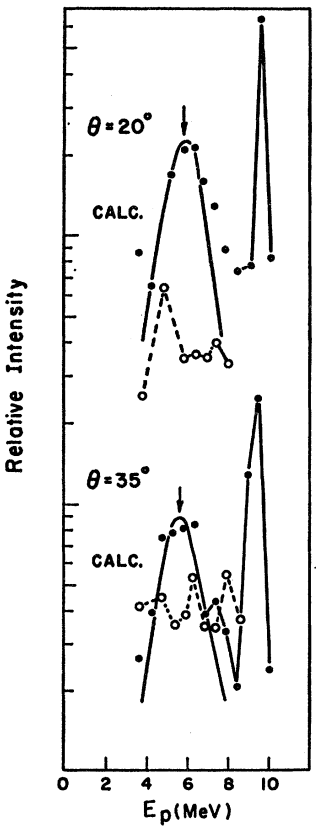


FIG. 8. Typical data from $(p, \bar{d})$ reactions on $C^{13}$ induced by 17-MeV protons. Open circles connected by the dashed line show opposite-side data. Solid curve is calculated energy distribution of protons. The high-energy peak is explained in the text.

[9] B. L. Cohen, E. Newman, T. H. Handley, and A. Timnick, Phys. Rev. 90, 323 (1953).

### 2. $C^{13}(p, \bar{d})C^{12}$

The $C^{13}(p, \bar{d})C^{12}$ reaction leading to the ground state of $C^{12}$ was studied at 17-MeV bombarding energy. A $C^{13}$ target was prepared by suspending over a mylar foil a sample of amorphous carbon with 50% enrichment in $C^{13}$ in an acetone-urethane solution, and allowing the acetone to evaporate. Since the target contains a large amount of nonuniformly distributed $C^{12}$, the usual monitoring technique is not applicable; instead, the monitor was set to detect the ground-state transition deuterons from the $C^{13}(p, d)C^{12}$ reaction. Figure 8 shows some typical data: The solid points are for the detectors on the same side of the beam, the usual $\bar{d}$ detection scheme, and the open circles are the opposite-side data. The latter are lower in intensity and are not peaked at $\frac{1}{2}E_0$, so our method for determining $(p, pn)$ background seems to work again here. The spectral shape also fits reasonably well to the calculated one shown by the solid curve. The angular distribution of $\bar{d}$ obtained from these data is shown in Fig. 9 where it is compared with that from the analogous $(p, d)$ reaction. The $\bar{d}$ angular distribution is clearly more isotropic; the fact that the $Q$ value is more negative than for $Be^9$ may partly explain this. There is some indication that the angular distribution is peaked at a larger angle for the $\bar{d}$ than for the $d$, as is expected.

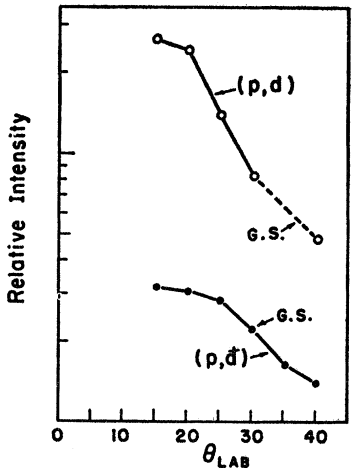


FIG. 9. Angular distribution of $d$ and $\bar{d}$ from $(p, d)$ and $(p, \bar{d})$ reactions on $C^{13}$ induced by 17-MeV protons and leading to the ground state of $C^{12}$.

It is interesting to note from Fig. 8 that there is a sharp peak in the energy spectrum at $E_p \simeq 9.3$ MeV.

This is due to the reaction

$$C^{13}(p, p')C^{13*}(7.68\ \text{MeV})$$
$$C^{13*} \rightarrow C^{12} + n.$$

The 7.68-MeV state of $C^{13}$ is strongly excited by $C^{12}(d, p)$ via a $d_{3/2}$ neutron transfer process[10] which indicates that its wave function is largely $C^{12}$ plus a $d_{3/2}$ single particle. Since the ground state of $C^{13}$ is largely $C^{12}$ plus a $p_{1/2}$ single particle, the $(p, p')$ process is essentially an excitation of the neutron from $p_{1/2}$ to $d_{3/2}$.

### 3. $Li^7(p, \tilde{d})Li^6$

The $Li^7(p, \tilde{d})Li^6$ reaction was studied at an incident proton energy of 12 MeV for transitions leading to the ground state of $Li^6$. Figure 10 shows typical spectra for the same-side case (closed points), the opposite-side case (open circles), and from the calculation of Appendix A (cashed curve). At all angles, the intensity for the opposite-side case is *larger* than for the same-side case, so the method of subtracting $(p, pn)$ background used with such apparent success for Be is not applicable here, and the interpretation of this data in terms of $(p, \tilde{d})$ is suspect. On the other hand, the spectra for the same-side case is peaked at the proper energy and has about the correct width, so an analysis in terms of $\tilde{d}$ was made. The angular distribution thus obtained is shown in Fig. 11, where it is compared with the angular distribution of ordinary deuterons, from the analogous $(p, d)$ reaction. There is a reasonable correspondence between the $d$ and $\tilde{d}$ angular distributions, although the one for $\tilde{d}$ is more isotropic. This may be explained by the rather large negative $Q$ value for the reaction coupled with the low bombarding energy. These data may also explain the large $d/\tilde{d}$ ratio $R$ listed in Table II for this reaction. The fact that this ratio is so large supports the interpretation of these data as due to $(p, \tilde{d})$ reactions rather than $(p, pn)$. The angular distribution of intensity in opposite-side runs is also shown in Fig. 11; it is not impossible that it is partly due to singlet deuterons, although no calculations were made on this.

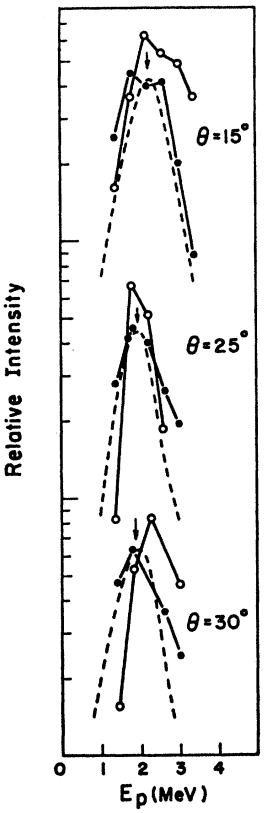


FIG. 10. Typical data from $(p, \tilde{d})$ and $(p, pn)$ reactions on $Li^7$ induced by 12-MeV protons. Solid points are same-side $(\tilde{d})$ data and open circles are opposite-side $(p, pn)$ data. Dashed curves are theoretically expected energy spectra and arrows show expected location of peak.

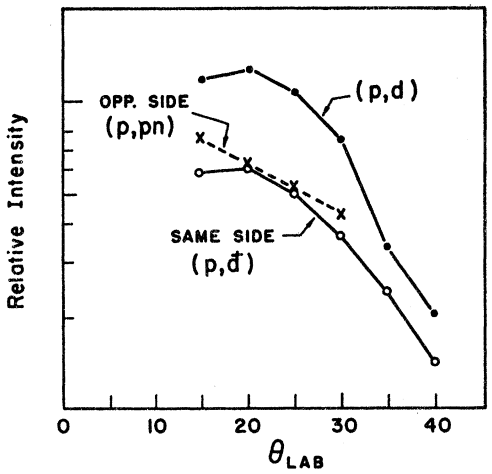


FIG. 11. Angular distributions obtained from data in Fig. 10, compared with angular distributions of deuterons from $(p, d)$ reactions.

### 4. $Mg^{25}(p, \tilde{d})Mg^{24}$

Data were taken on the $Mg^{25}(p, \tilde{d})$ reaction leading to both the ground and 1.3-MeV states of $Mg^{24}$. In this target, the $(p, pn)$ cross section is extremely high, especially for transitions to the 1.3-MeV state. The peaks of the proton energy spectra are at much higher energy than $\frac{1}{2}E_0$, but the intensity at $\frac{1}{2}E_0$ is still sufficiently high that effects from singlet deuterons are completely masked. The rather small lower limits on $R$ in Table II indicate that the expected intensity of $\tilde{d}$'s is too small to be observable.

### 5. $Sn^{119}(p, \tilde{d})Sn^{118}$

Since interference from $(p, pn)$ reactions was found to be so important in Mg, there seemed to be an advantage in skipping to a target nucleus so heavy that

[10] J. N. McGruer, E. R. Warburton, and R. S. Bender, Phys. Rev. **100**, 235 (1955).

no protons from $(p, pn)$ reactions are expected in the energy region near $\frac{1}{2}E_0$ because of the Coulomb barrier. Since the $\bar{d}$ is formed far outside the nucleus, it might be hoped that its emission would not be strongly suppressed by the Coulomb barrier. In order to test this, a $Sn^{119}$ target was chosen because it has a favorable atomic number and $Q$ value, and the pickup reaction leading to the ground state of $Sn^{118}$ is known to have a large cross section[11] and an angular distribution peaked at a favorable angle ($\sim 30°$).

The spectra obtained have been published in another connection,[12] but they have no observable intensity at energies near $\frac{1}{2}E_0$. The upper limit on this intensity gives a very high lower limit on $R$ as listed in Table II. This might be explained by the large negative $Q$ value and the high Coulomb barrier. It is also possible that the large Coulomb barrier distorts the proton spectrum from singlet deuteron breakup and moves its peak to higher energy; if this explanation is correct, the value of $R$ listed in Table II should be very much reduced.

## CONCLUSIONS

The method described at the beginning of this paper for detecting singlet deuterons and studying reactions in which they are products works very well for $Be^9(p, \bar{d})$ at 17-MeV as well as at 12-MeV bombarding energy, and seems to work also for $C^{13}(p, \bar{d})$ and perhaps for $Li^7(p, \bar{d})$. Meaningful angular distributions of $\bar{d}$'s are obtained, and they are similar to analogous angular distributions of ordinary deuterons, with the differences being approximately as predicted. The intensity of $\bar{d}$'s is also of the expected magnitude. For all other target nuclei there are great difficulties, but it should be pointed out that the maximum energy available in these experiments was only 17 MeV which is quite marginal for all target nuclei except $Be^9$. With higher bombarding energies, differences between $(p, d)$ and $(p, \bar{d})$ should be much less and many other nuclei could be studied.

All things considered, it is feasible to use $\bar{d}$ as a nuclear reaction product, but experimental difficulties are appreciable and the accelerator times required are long; such uses should be limited to cases where a great deal of important information can be obtained with a relatively few measurements.

It is hoped that the $(p, d)/(p, \bar{d})$ ratios $R$ from Table II and the angular distributions from Figs. 7, 9, and 11 will be useful to theorists in further analysis of these reactions

## APPENDIX A: CALCULATION OF PROTON ENERGY SPECTRUM AND EFFICIENCY FOR $\bar{d}$ DETECTION

We consider a $\bar{d}$ to come off with velocity $\mathbf{v}$, and to break up into a neutron and a proton, which come off with velocities $\mathbf{u}$ and $-\mathbf{u}$ relative to the $\bar{d}$ center of mass. The angle between $\mathbf{u}$ and $\mathbf{v}$ is $\phi$. In terms of these, the energies, as given by (1), are

$$\begin{aligned} &E_{\bar{d}}+E_{\mathrm{BU}}=E_0, \text{ a known const},\\ &E_{\bar{d}}=mv^2,\\ &E_{\mathrm{BU}}=mu^2, \qquad\qquad (A1)\\ &E=\tfrac{1}{2}m[(v+u\cos\phi)^2+(u\sin\phi)^2]. \end{aligned}$$

In determining $E_0$, $E_{\mathrm{recoil}}$ is calculated under the assumption that $v \gg u$ for reasons given in the Introduction; actually, this makes little difference. It is easily shown by simple geometry that the angle $\alpha$ in the laboratory system between the neutron and the proton is given by

$$\sin\phi=[(u/2v)-(v/2u)]\tan\alpha. \qquad (A2)$$

We take the diameter of the proton detector to be very small, so the maximum angle $\alpha$ for which both the neutron and proton reach their detectors, $\alpha_m$, is the half-angle subtended by the neutron detector. The angle $\phi_m$ is then obtained by inserting $\alpha_m$ into (A2); it is a function of $E_{\mathrm{BU}}$ throughout Eq. (A1).

The calculation of the energy spectrum of protons (or neutrons) then proceeds by breaking $E_{\mathrm{BU}}$ and $\phi$ into small finite intervals, $\Delta E_{\mathrm{BU}}$ and $\Delta\phi$. For each combination of $E_{\mathrm{BU}}$ and $\phi$, the nucleon energy $E_n$ is calculated from the last of Eq. (A1). This combination contributes a weight $\frac{1}{2}\sin\phi(\Delta\phi)P(E_{\mathrm{BU}})\Delta E_{\mathrm{BU}}$ to that value of $E_n$ *provided* $\phi$ is less than $\phi_m$; the first factor is obtained by integration over azimuthal angles and normalizing, and $P(E_{\mathrm{BU}})$ is obtained from the density-of-states function, as will be described in the next paragraph. When all combinations of $\phi$ and $E_{\mathrm{BU}}$ have been considered, the contributions to the weights of all $E_n$ within equal finite intervals $\Delta E_n$ are summed, and this process is carried out over the entire range of $E_n$ to give the energy spectrum of neutrons or protons. The sum over this spectrum gives the "efficiency for $\bar{d}$ detection" which we define as the probability that the neutron will reach its detector *if* the proton reaches its detector. The actual detection efficiency is the product of this efficiency and the efficiency of the neutron detector for responding to neutrons which strike it. In calculations of detection probabilities, the solid angle for the $\bar{d}$ detector is taken as the solid angle subtended by the proton detector times this "actual" efficiency.

The factor $P(E_{\mathrm{BU}})$ is obtained as follows: From Ref. 12, the density-of-states function is proportional to

$$(1/k)[(d/dk)(\delta+ka_1)-(1/2k)\sin 2(\delta+ka_1)], \qquad (A3)$$

where $k=(2mE_n/\hbar^2)^{1/2}$ is the nucleon wavenumber, $\delta$ is the phase shift in $n$-$p$ scattering in the singlet state, and $a_1$ is the range of the interaction between the $\bar{d}$ and the residual nucleus. From the well-known relationship

$$k\cot\delta=-(1/a)+\tfrac{1}{2}r_0k^2,$$

[11] B. L. Cohen and R. E. Price, Phys. Rev. **121**, 1441 (1961).
[12] B. L. Cohen, E. C. May, T. M. O'Keefe, C. L. Fink, and B. Rosner, Phys. Rev. Letters **21**, 226 (1968).

where $a$ is the scattering length and $r_0$ is the effective range in singlet $n$-$p$ scattering, the derivative needed in (A3) is

$$d\delta/dk=[(1/k^2a)+\tfrac{1}{2}r_0]\sin^2\delta. \quad \text{(A4)}$$

In order to determine $P(E_{\mathrm{BU}})$, Eq. (A3) should be multiplied by the density of states in the continuum for the motion of the $\hat{d}$, which is proportional to $(E_0-E_{\mathrm{BU}})^{1/2}$. Using this and (A4) in (A3) gives

$$P(E_{\mathrm{BU}})=(B/k^2)\{ka_1-[(1/ka)+\tfrac{1}{2}r_0k]\times\sin^2\delta-\tfrac{1}{2}\sin2(\delta+ka_1)\}(E_0-E_{\mathrm{BU}})^{1/2}.$$

This was evaluated for $a=-23.8$ F$^{-1}$, $r_0=2.49$ F, and various values of $a_1$; fortunately, the results are fairly independent of $a_1$ for all reasonable values—between 1 and 10 F. The factor $B$ is chosen to normalize the integral $\int_0^{E_0} PdE$ to unity.

## ACKNOWLEDGMENTS

The authors would like to acknowledge many helpful discussions with K. Nagatani, E. W. Hamburger, J. X. Saladin, N. Austern, F. Tabakin, and S. Gangadharan.

PHYSICAL REVIEW VOLUME 179, NUMBER 4 20 MARCH 1969

# Study of $\alpha+d$ and $\alpha+d^*$ Systems with the Resonating-Group Method†

D. R. Thompson‡ and Y. C. Tang

*School of Physics, University of Minnesota, Minneapolis, Minnesota 55455*

(Received 27 November 1968)

The resonating-group method with a one-channel approximation is used to examine the $\alpha+d$ elastic scattering and bound-state problems. The nucleon-nucleon potential employed is the same as that used in previous resonating-group calculations and fits the low-energy scattering data satisfactorily. The deuteron wave function, which is given by a sum of two Gaussian functions, yields nearly correct values for the binding energy and the rms radius. For the bound and resonant states in $Li^6$, it is shown that a careful consideration of the distortion effect on the deuteron cluster is essential. The calculated excitation energy of the $^3D$ level is 4.6 MeV, which is rather close to the value of 3.8 MeV obtained by averaging the excitation energies of the experimentally found $^3D_3$, $^3D_2$, and $^3D_1$ levels. Phase shifts are calculated in the energy region of 0–20 MeV and, in general, they agree quite well with those determined phenomenologically. In particular, the result shows that in the excitation region below 10 MeV, the $P$-wave phase shifts are small and show no resonance behavior. The $T=1$ levels in the isobaric triad $He^6$, $Li^6$, and $Be^6$, which have predominantly a structure of an $\alpha$ cluster plus a two-nucleon cluster in a $^1S_0$ configuration ($d^*$ cluster), have also been studied. Here it is found that with a two-Gaussian function for the $d^*$ cluster, the calculated energy spacings between the $^1S$ and the $^1D$ levels are too large by about 1 MeV.

## I. INTRODUCTION

In a recent investigation,[1] the elastic scattering of deuterons by $\alpha$ particles has been studied with the resonating-group method in the one-channel approximation. In that study, the calculation was simplified by introducing the assumption that the deuteron cluster can be described by a single-Gaussian function, with its width parameter adjusted to yield the correct rms radius of a free deuteron. With this assumption and a properly chosen exchange mixture in the nucleon-nucleon potential, it was found that the essential features of the $d+\alpha$ elastic scattering can be explained; in particular, the calculation correctly predicted the nonresonant nature of the $P$-wave phase shifts and the existence of a $D$-wave resonance in the low-energy region.[2–6]

Even though the results obtained with the single-Gaussian approximation for the deuteron eigenfunction were fairly satisfactory, a careful examination did reveal that there was one undesirable feature in the calculation. To obtain the correct separation energy of the deuteron cluster in the ground state of $Li^6$, it was found necessary to adjust the exchange mixture until the nucleon-nucleon interaction in the odd orbital-angular-momentum states becomes much more attrac-

† Work supported in part by the U.S. Atomic Energy Commission.

‡ Present address: California Institute of Technology, Pasadena, Calif. 91109.

[1] D. R. Thompson and Y. C. Tang, Phys. Letters **26B**, 194 (1968).

[2] L. S. Senhouse, Jr. and T. A. Tombrello, Nucl. Phys. **57**, 624 (1964).

[3] L. C. McIntyre and W. Haeberli, Nucl. Phys. **A91**, 382 (1967).

[4] P. Darriulat, D. Garreta, A. Tarrats, and J. Arvieux, Nucl. Phys. **A94**, 653 (1967).

[5] T. Lauritsen and F. Ajzenberg-Selove, Nucl. Phys. **78**, 1 (1966).

[6] P. E. Shanley, Phys. Rev. Letters **21**, 627 (1968).